Pure appl. geophys. 166 (2009) 153–175
0033–4553/09/010153–23
DOI 10.1007/s00024-008-0435-4

Pure and Applied Geophysics

Lituya Bay Landslide Impact Generated Mega-Tsunami 50th Anniversary

HERMANN M. FRITZ, FAHAD MOHAMMED, and JESEON YOO

Abstract—On July 10, 1958, an earthquake M_w 8.3 along the Fairweather fault triggered a major subaerial landslide into Gilbert Inlet at the head of Lituya Bay on the southern coast of Alaska. The landslide impacted the water at high speed generating a giant tsunami and the highest wave runup in recorded history. The mega-tsunami runup to an elevation of 524 m caused total forest destruction and erosion down to bedrock on a spur ridge in direct prolongation of the slide axis. A cross section of Gilbert Inlet was rebuilt at 1:675 scale in a two-dimensional physical laboratory model based on the generalized Froude similarity. A pneumatic landslide tsunami generator was used to generate a high-speed granular slide with controlled impact characteristics. State-of-the-art laser measurement techniques such as particle image velocimetry (PIV) and laser distance sensors (LDS) were applied to the decisive initial phase with landslide impact and wave generation as well as the runup on the headland. PIV provided instantaneous velocity vector fields in a large area of interest and gave insight into kinematics of wave generation and runup. The entire process of a high-speed granular landslide impact may be subdivided into two main stages: (a) Landslide impact and penetration with flow separation, cavity formation and wave generation, and (b) air cavity collapse with landslide run-out and debris detrainment causing massive phase mixing. Formation of a large air cavity — similar to an asteroid impact — in the back of the landslide is highlighted. A three-dimenional pneumatic landslide tsunami generator was designed, constructed and successfully deployed in the tsunami wave basin at OSU. The Lituya Bay landslide was reproduced in a three-dimensional physical model at 1:400 scale. The landslide surface velocities distribution was measured with PIV. The measured tsunami amplitude and runup heights serve as benchmark for analytical and numerical models.

Key words: Tsunami, landslide, landslide generated tsunami, natural hazard, nonlinear gravity water waves, wave runup, near-field wave characteristics, slide energy conversion, three-phase flow, Alaska.

1. Introduction

Lituya Bay is a T-shaped tidal inlet that cuts through the coastal lowlands and the foothills flanking the Fairweather Range of the St. Elias Mountains on the southern coast of Alaska shown in Figure 1a. The stem corresponding to the main part of the T-shaped bay is 12 km long and extends northeastward from the bay entrance. The width of the stem ranges from 1.2 to 3.3 km except at the entrance, which is only 300 m wide. The bay fills and slightly overflows a depression carved by a valley glacier of which Lituya, North Crillon and Cascade glaciers are remnants. Submarine contours show a pronounced

School of Civil and Environmental Engineering, Georgia Institute of Technology, 210 Technology Circle, Savannah, GA 31407, U.S.A. E-mail: fritz@gatech.edu

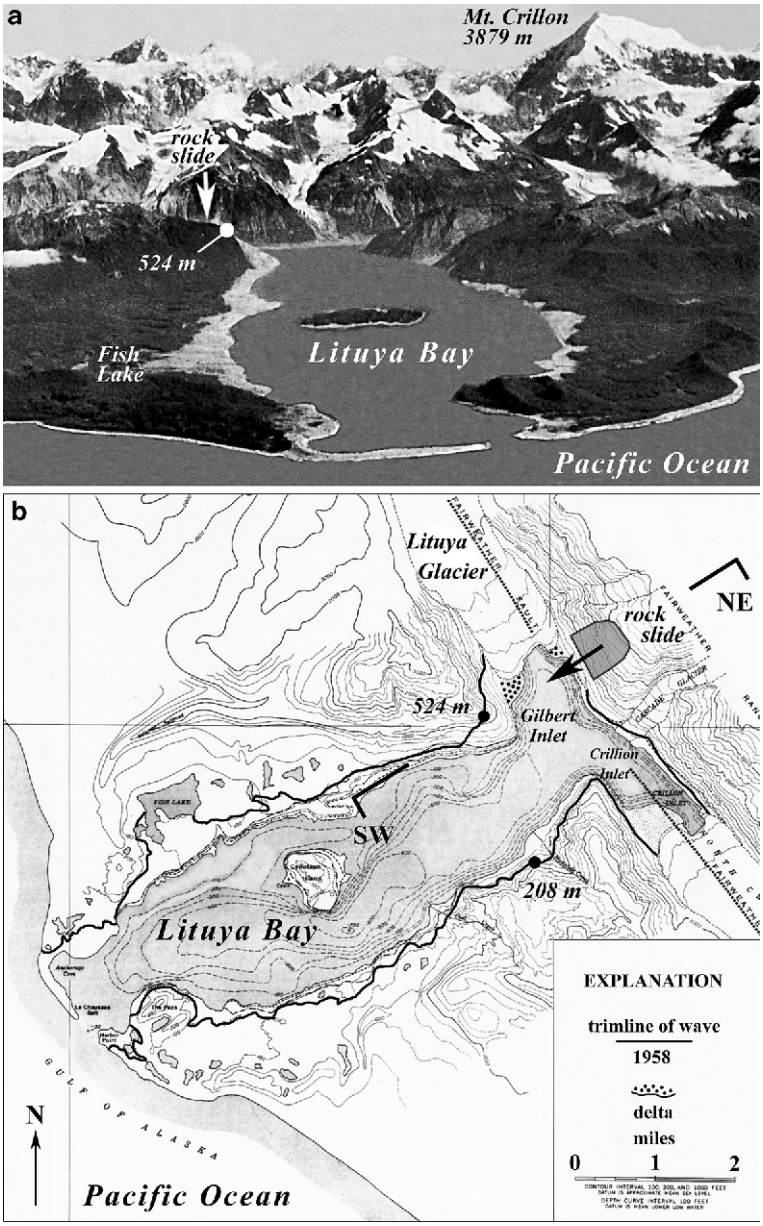

Figure 1

Lituya Bay, Alaska: (a) Overview in August 1958 (MILLER, 1960). Forest destroyed to a maximum elevation of 524 m and a maximum distance of 1100 m from high-tide shoreline at Fish Lake due to a giant tsunami generated on 10 July 1958 by a landslide at the head of the bay. (b) Map showing topographic and bathymetric contours, trace of Fairweather fault, 1958 landslide and trimline of tsunami runup (MILLER, 1960).

U-shaped trench with steep walls and a broad flat floor sloping gently downward from the head of the bay to a maximum depth of 220 m. Minimum depth at the entrance of the bay is 10 m. At the head of the bay the walls are fjord-like glacially over-steeped. The walls have been buttressed by glaciers until recently. Radiocarbon dates on high moraines suggest retreat of glaciers only in the last millennium (SLINGERLAND and VOIGHT, 1979). The two arms at the head of the bay are part of a great trench that extends tens of kilometers to the northwest and southeast as a topographic expression of the Fairweather transform fault shown in Figure 1b.

Giant waves have occurred in Lituya Bay probably five times during the last two centuries emphasizing the unique geologic and tectonic setting of the bay. Frequent occurrence of giant waves in Lituya Bay, as compared to other similar bays, is attributed to the combined effect of recently glaciated steep slopes, highly fractured rocks and deep water in an active fault zone, heavy rainfall, frequent freezing and thawing (MILLER, 1960). Three extreme wave runup heights in 1853 or 1854, 1936 and 1958 carved sharp trimlines of chopped trees to elevations beyond 100 m on to the slopes of Lituya Bay. Photographic evidence and eyewitness accounts suggest two additional giant waves occurred possibly in 1874 and 1899 (MILLER, 1960). In 1853 or 1854 a giant wave caused forest destruction on Lituya Bay shores to a maximum elevation of 120 m. A landslide from the steep wall on the south shore of Lituya Bay near Mudslide Creek is the likely source directly opposite to the maximum destruction on the north shore. The trimline of the 1936 waves reached a maximum height of 150 m above sea level on the northeast wall of Crillon Inlet and indicates a wave generation near the head of Crillon Inlet. MILLER (1960) suggests a landslide or rock avalanche from the southwest wall of Crillon Inlet, opposite the high point on the trimline. In 1958 the largest wave runup of 524 m in recorded history was observed on a spur ridge on the southwest wall of Gilbert Inlet. Only the 1958 event is further considered here as the exact sources of the earlier events remain to be confirmed by bathymetric and geologic surveys of the seafloor.

2. 1958 Landslide Impact and Tsunami Runup

Beginning at 06:16 UTC on July 10, 1958, the southwest sides and bottoms of Gilbert and Crillon Inlets moved northwestward and relative to the northeast shore at the head of the bay, on the opposite side of the Fairweather fault. Total movements of 6.4 m horizontally and 1 m vertically were estimated for the earthquake M_w 8.3 (TOCHER and MILLER, 1959). Intense shaking in Lituya Bay continued for 1 to 4 minutes according to two eyewitnesses that anchored in the bay. Between 1 and 2½ minutes after the earthquake was first felt a large mass of rock slid from the northeast wall of Gilbert Inlet (Fig. 2). The landslide was triggered impulsively by fault movement and intense earthquake vibrations. It is highly probable that the entire mass plunged into Gilbert Inlet as a unit at the time of the earthquake. PARARAS-CARAYANNIS (1999) classified the mass movement as subaerial rockfall to distinguish from gradual processes of ordinary

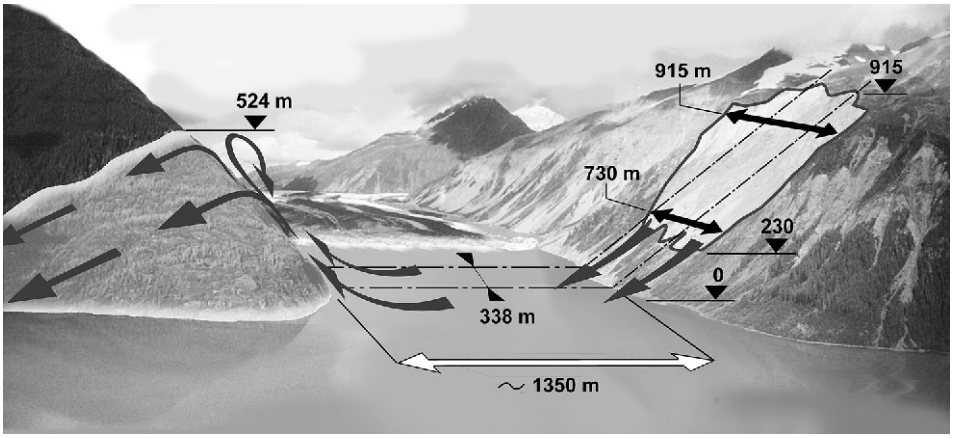

Figure 2
Gilbert Inlet illustration showing landslide dimensions, impact site and tsunami runup to 524 m on spur ridge directly opposite to landslide impact. Direction of view is north and the front of Lituya Glacier is set to 1958 post-slide position. Illustration background is synthesized from two aerial photos recorded in 1997 (Photos: courtesy of Charles L. Mader).

landslides whereas MILLER (1960) judged it to be near the borderline between landslide and rockfall as defined by SHARPE (1938) and VARNES (1958). The landslide occurred in an area of previously active sliding to an elevation of 915 m on a slope averaging 40°. The rocks are mainly amphibole and biotite schists with an estimated density of 2.7 t/m^3. The dimensions of the slide on the slope are accurate, but the thickness of the slide mass normal to the slope could be estimated only roughly (MILLER, 1960). The main mass of the slide presumably involved a prism of rock roughly triangular in cross section, with width dimensions from 730 m to 915 m (MILLER, 1960; SLINGERLAND and VOIGHT, 1979), a slope parallel length of 970 m (SLINGERLAND and VOIGHT, 1979), a maximum thickness of about 92 m normal to the slope, and a center of gravity at about 610 m elevation (MILLER, 1960). Dimensions are illustrated in Figure 2. Miller estimated the slide volume from these as 30.6×10^6 m^3.

Prior to the landslide low deltas of gravel had built out into Gilbert Inlet at the southeast and northwest margins of the Lituya Glacier front. Part of the slide must have hit the Lituya Glacier and glacial gravel deltas due to the pre-slide location of slide mass, deltas and glacier front (MILLER, 1960). The Lituya Glacier front was characterized by a vertical wall normal to the Gilbert Inlet axis after the event (Figs. 3a, b). During the event as much as 400 m of ice had been sheared off on parts of the glacier front and the gravel deltas were pushed or washed away. The landslide impact created a giant tsunami and a resulting maximum tsunami runup of 524 m in straight prolongation of the slide axis on a spur ridge on the southwest shore of Gilbert Inlet (Figs. 3a, b, c).

The maximum tsunami runup of the 1958 event was incomparable at the time to any other event outside of Lituya Bay. The 524 meter runup is seven times larger than

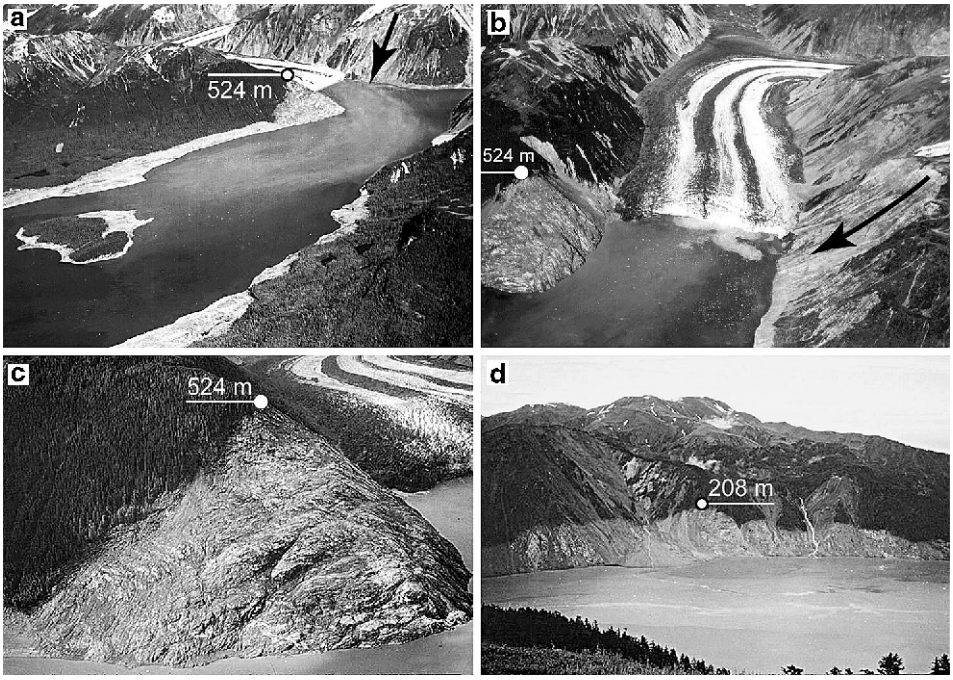

Figure 3
Trimlines carved by tsunami in 1958: (a) NE-view of Lituya Bay from Cenotaph Island to Gilbert Inlet with landslide scar at the head of the bay and trimlines of destructed forest with 524 m runup on spur ridge. (b) NW-view of Gilbert Inlet with landslide scar, post-event Lituya Glacier front, forest destruction and soil erosion down to bedrock. (c) N-view of spur ridge. (d) S-view of trimline in the Mudslide Creek area on the south shore of Lituya Bay with wiped out trees to an elevation of 208 m. (Photos: courtesy of USGS).

the highest tsunami runup of 75 m observed 1936 in Norwegian Lake Loen (JØRSTAD, 1968) and roughly doubles wave runup heights in the Vajont reservoir, Italy (MÜLLER, 1964) and Spirit Lake, U.S.A. (VOIGHT *et al.*, 1983). A simplified 3-D physical model of Lituya Bay at a 1:1,000 scale was constructed at the University of California, Berkeley (R.L. WIEGEL in MILLER, 1960, pp. 65-66). Wiegel concluded from physical model observations, that a sheet of water washed up the slope opposite to the landslide to an elevation of at least three times the water depth for a slide impacting Gilbert Inlet as a unit and very rapidly. At the same time a large wave, several hundred feet high, moved in the southerly direction, causing a peak rise to occur in the vicinity of Mudslide Creek. Unfortunately no measured data are available from these three dimensional experiments. The highest mark of chopped trees at an elevation of 208 m on the south shore trimline is shown in Figure 3d. WIEGEL (1964) estimated the hydrodynamic forces exerted on the trees by the wave as roughly ten times greater than the force necessary to snap or uproot trees.

3. Physical Model of Gilbert Inlet

Based on the generalized Froude similarity a cross section of Gilbert Inlet was rebuilt at a 1:675 scale in a two-dimensional physical laboratory model (L × W × H: 11 m, 0.5 m and 1 m) by FRITZ *et al.*, 2001. The Froude similarity has been confirmed by a laboratory scale series (HELLER *et al.*, 2008). The modeled Gilbert Inlet cross section is shown in Figure 4a and its NE-SW orientation in Figure 1b. The prismatic Gilbert Inlet slice rebuilt in the model is shown in Figure 2. The width of 338 m represented in the 2-D model corresponds to 40% of the mean slide width of 823 m (SLINGERLAND and VOIGHT, 1979). The volume per unit width $V_s' = 37.2 \times 10^3$ m^3/m$'$ was estimated by equal distribution of the total slide volume $V_s = 30.6 \times 10^6$ m^3 over an averaged slide width of 823 m. This is a conservative assumption neglecting the volume concentration in the slide center due to roughly triangular slide cross sections along the slope. The indicated geometry corresponds to the physical model assumptions with a hill slope angle α and a headland angle β of both 45°. The simplified Gilbert Inlet bathymetry roughly corresponds to bedrock of the glacially carved U-shaped trench. Pre-slide gravel deltas

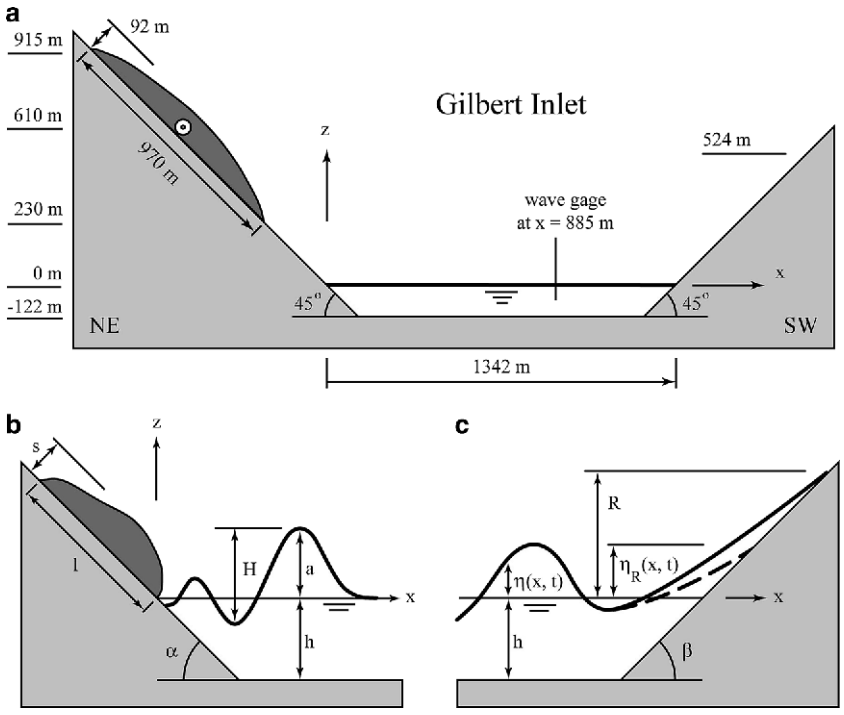

Figure 4
(a) Cross section of Gilbert Inlet along slide axis in NE to SW orientation shown in Figure 1b. Geometry corresponds to physical model assumptions and simplifications. (b) Notation for landslide impact and wave propagation; (c) notation for wave runup.

along parts of the glacier front shown in Figure 1b were neglected. The assumed stillwater depth $h = 122$ m matches the maximum water depth in Gilbert Inlet. The notation for landslide impact, wave propagation and wave runup are defined (Figs. 4b, c).

Radial or lateral wave spreading is neglected in the two-dimensional model. In northern direction the impact area is confined to the Lituya Glacier front. In this specific topographic situation wave height reduction due to 3-D effects is further limited by the small ratio of 1.6 between propagation distance and slide width. Therefore it is expected that the present 2-D model can give a good estimate of wave and runup heights in Gilbert Inlet.

The dynamic slide impact characteristics were controlled with a specifically designed pneumatic landslide generator shown in Figure 5 (FRITZ and MOSER, 2003). The pneumatic landslide generator models the transition from block slide motion to granular flow. The first stage with acceleration up to the granulate release velocity corresponds to block sliding whereas the second stage from granulate release to impact into the water body is purely gravity driven granular flow.

Three different measurement techniques were built into the physical model: Laser distance sensors (LDS), particle image velocimetry (PIV) and capacitance wave gauges

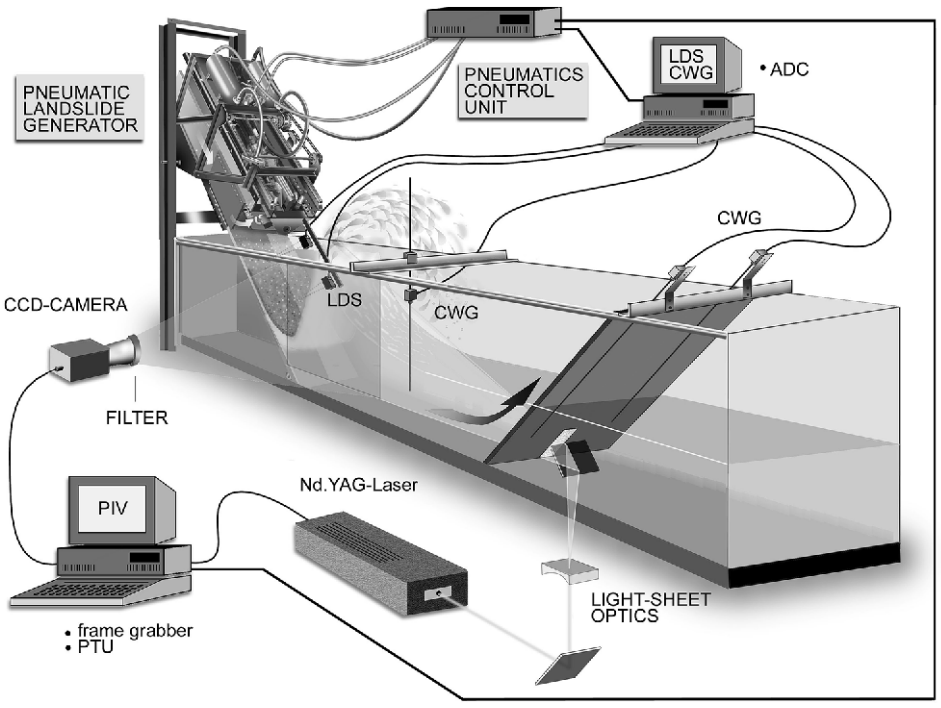

Figure 5
Experimental setup with pneumatic installation and measurement systems: Laser distance sensors (LDS), capacitance wave gages (CWG) and particle image velocimetry (PIV).

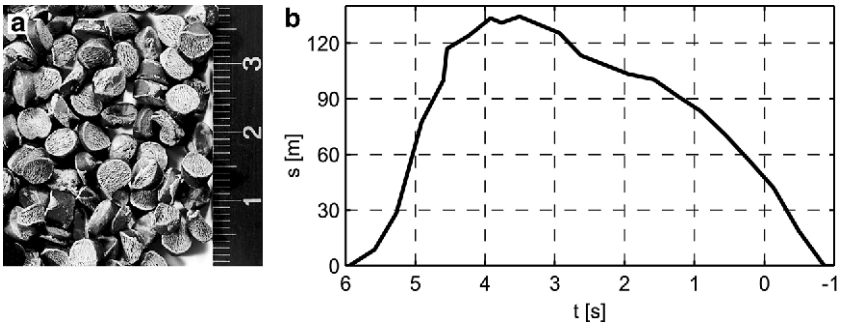

Figure 6
(a) Granulate: PP-$BaSO_4$, $d_g = 4$ mm, $\rho_g = 2.64$ g/cm^3; (b) granular slide profile scanned with a laser distance sensor orthogonal to ramp at location $x = -67$ m and $z = 67$ m.

(CWG). The laser-based digital PIV-system was introduced in FRITZ (2002a). The planar PIV provided instantaneous velocity vector fields in the slide impact area and gave insight into the kinematics of wave generation (FRITZ *et al.*, 2003a). Water displacement volumes and rates were extracted from the PIV recordings (FRITZ *et al.*, 2003b). Instantaneous image areas as large as 529(H) × 516(V) m in prototype scale were acquired. By means of cross-correlation analysis instantaneous 2D-2C velocity vector fields were computed using an adaptive multi-pass algorithm (SCARANO and RIETHMULLER, 1999) and second-order correlation (HART, 2000). Spatial resolution is determined by the window size of 8.4 × 8.4 m used in cross-correlation analysis. Time resolution of the PIV-system for 2D-2C velocity vector field estimation was 0.6 Hz in prototype time scale.

The landslides were modeled with an artificial granular material (PP-$BaSO_4$) shown in Figure 6a. The granulate properties were: grain density $\rho_g = 2.64$ t/m^3, grain diameter $d_g = 4$ mm, bulk slide density $\rho_s = 1.62$ t/m^3, bulk slide porosity $n_{\text{por}} = 39\%$, effective internal friction angle $\phi' = 43°$, and dynamic bed friction angle $\delta = 24°$ (FRITZ, 2002b). The slip between the bed and the granular mass was dominant, resulting in slug-type flow (SAVAGE, 1979). Its grain density perfectly matches the estimated schist density of $\rho_s = 2.7$ t/m^3 and resulted in a slide mass per unit width of $m' = 98.5 \times 10^3$ t/m′. The assumed porosity corresponds to data from Alpine debris flows (TOGNACCA, 1999). Slide profiles before impact are scanned with two laser distance sensors. A landslide profile recorded orthogonal to the ramp and 67 m above the stillwater level is shown in Figure 6b. The maximum slide thickness of 134 m equals 1.4 times the pre-motion slide thickness of 92 m (MILLER, 1960). This increase of 40% in slide thickness is necessary in the model to compensate for the void fraction present in granular flow in order to match the slide mass-flux per unit width. The prototype landslide porosity likely also increased due to fragmentation of the schist slide mass prior to impact. The generated slide length before impact was conservatively estimated to 748 m with the mean slide velocity of 110 m/s and the slide profile duration of 6.8 s. The mean landslide impact velocity v_s of

110 m/s is estimated assuming free fall equations for a slide centroid at 610 m elevation (LAW and BREBNER, 1968; NODA, 1970). The kinetic impact energy of the landslide is at the upper limit neglecting frictional losses. This gives an impact slide Froude number of 3.18 based on the definition $F = v_s/(gh)^{1/2}$. The slide Froude number relates the mean impact velocity v_s of the centroid to the shallow water wave propagation velocity (NODA, 1970). Scale effects regarding viscosity and surface tension may be assumed smaller than 5% (STIVE, 1985; MÜLLER, 1995).

Wave features during propagation and runup are determined with capacitance wave gages (CWG). One CWG records the wave profile at $x = 885$ m and two CWGs record wave runup profiles on the headland ramp. Laser distance sensors and capacitance wave gauges are sampled at 20 Hz in prototype time scale (FRITZ *et al.*, 2001).

4. 2-Dimensional Experimental Results

A series of experiments was conducted with the assumptions for Lituya Bay topography, bathymetry, landslide impact velocity, mass and shape described in the physical model section. The waves generated by the granulate inflow (Fig. 6b) and recorded with a capacitance wave gauge at location $x = 885$ m are shown in Figure 7a. The wave propagating away from the impact area in positive x-direction creates a single initial peak at $t = 16$ s with a maximum positive amplitude $a = 152$ m. In the two-dimensional model of Gilbert Inlet the single outward travelling wave is reflected back and forth from both headland and landslide ramps. The main trailing peaks recorded on the wave gauge have altering propagation directions from positive to negative x-direction, respectively. The second peak ($a = 85$ m, $t = 48$ s) on the wave record corresponds to the wave reflection from the headland propagating in the negative x-direction. An experiment without the headland ramp showed that the first wave trough ($\eta = 37$ m, $t = 30$ s) is truncated by the reflection from the headland and not fully developed. In the experiment without headland ramp a flat trough with a negative amplitude $a = -10$ m was recorded behind the single outward travelling wave crest. Therefore the total wave height is estimated to $H = 162$ m. The measured wave height to stillwater depth ratio $H/h = 1.33$ is well beyond any breaking criterion (DEAN and DALRYMPLE, 1991). The experimental run without headland ramp showed that breaking and transformation to a nonlinear bore initiated roughly at $x = 1500$ m — after the beginning of the headland ramp at location $x = 1342$ m. The third main peak ($a = 111$ m, $t = 93$ s) and the fifth peak ($a = 57$ m, $t = 180$ s) correspond to the wave reflected back from the landslide slope. The fourth peak ($a = 73$ m, $t = 129$ s) and the sixth peak ($a = 57$ m, $t = 214$ s) are wave reflections from the headland ramp. This partial back and forth wave reflection in Gilbert Inlet could account for the "jumping and shaking" reported by one eyewitness (MILLER, 1960).

The corresponding wave runup recorded by a capacitance wave gage on the headland ramp is shown in Figure 7b. The runup gauge record acquired parallel to the 45° inclined

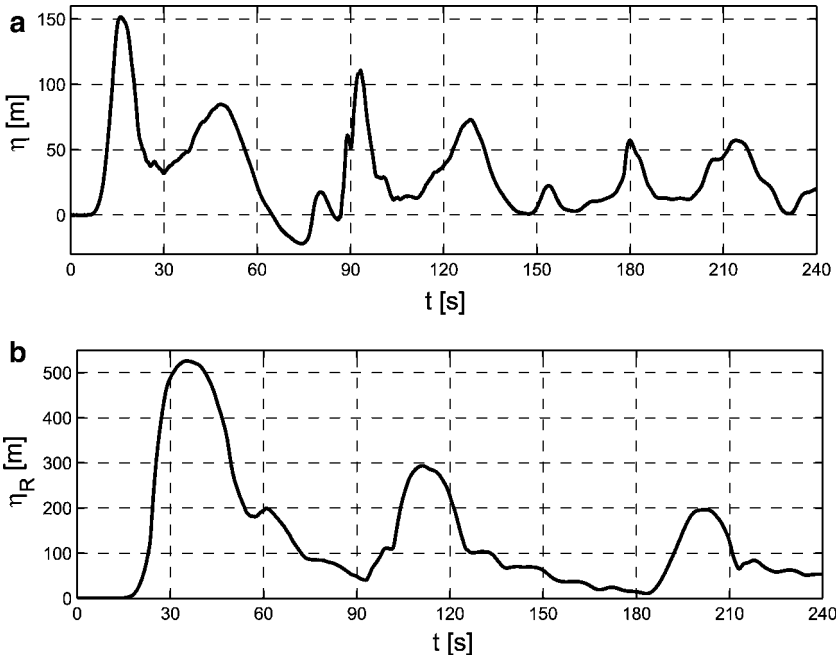

Figure 7
(a) Tsunami record at location $x = 885$ m; (b) tsunami runup record on headland ramp at locations $x = 1342$ m + η_R measured with capacitance wave gauges.

headland ramp is transformed into an elevation record. On the headland ramp a maximum runup height of $R = 526$ m is measured at $t = 35$ s. The measured runup of 526 m perfectly matches the highest elevation of 524 m on the trimline of forest destruction in Gilbert Inlet. The two trailing peaks on the runup record correspond to the first and second reflection of the single initial wave runup. The peak-to-peak period increases from 76 s to 91 s. This decay in propagation velocity with diminishing wave amplitude is due to the characteristic amplitude dispersion of nonlinear waves.

A sequence of twelve instantaneous velocity vector plots computed with PIV is shown in Figure 8. The sequence starts at t = 0.76 s after landslide impact and continues with a time step of 1.73 s covering roughly a time span of 20 s. Instantaneous velocity vector plots provide insight into kinematics during landslide impact and tsunami generation. The entire process may be subdivided into two main stages: (a) Slide impact and penetration (Fig. 8a), flow separation (Fig. 8b), cavity formation (Figs. 8c, d, e, f) while slide penetration velocity exceeds wave propagation velocity, and (b) cavity collapse (Figs. 8g, h), slide run-out along channel bottom, slide detrainment and deposition (Figs. 8i, j, k, l) as the wave overtakes the landslide and propagates out of the impact area. At the beginning of the cavity collapse (Fig. 8g) the splash amplitude exceeds 200 m in elevation at $x = 600$ m and $t = 11.14$ s before decaying

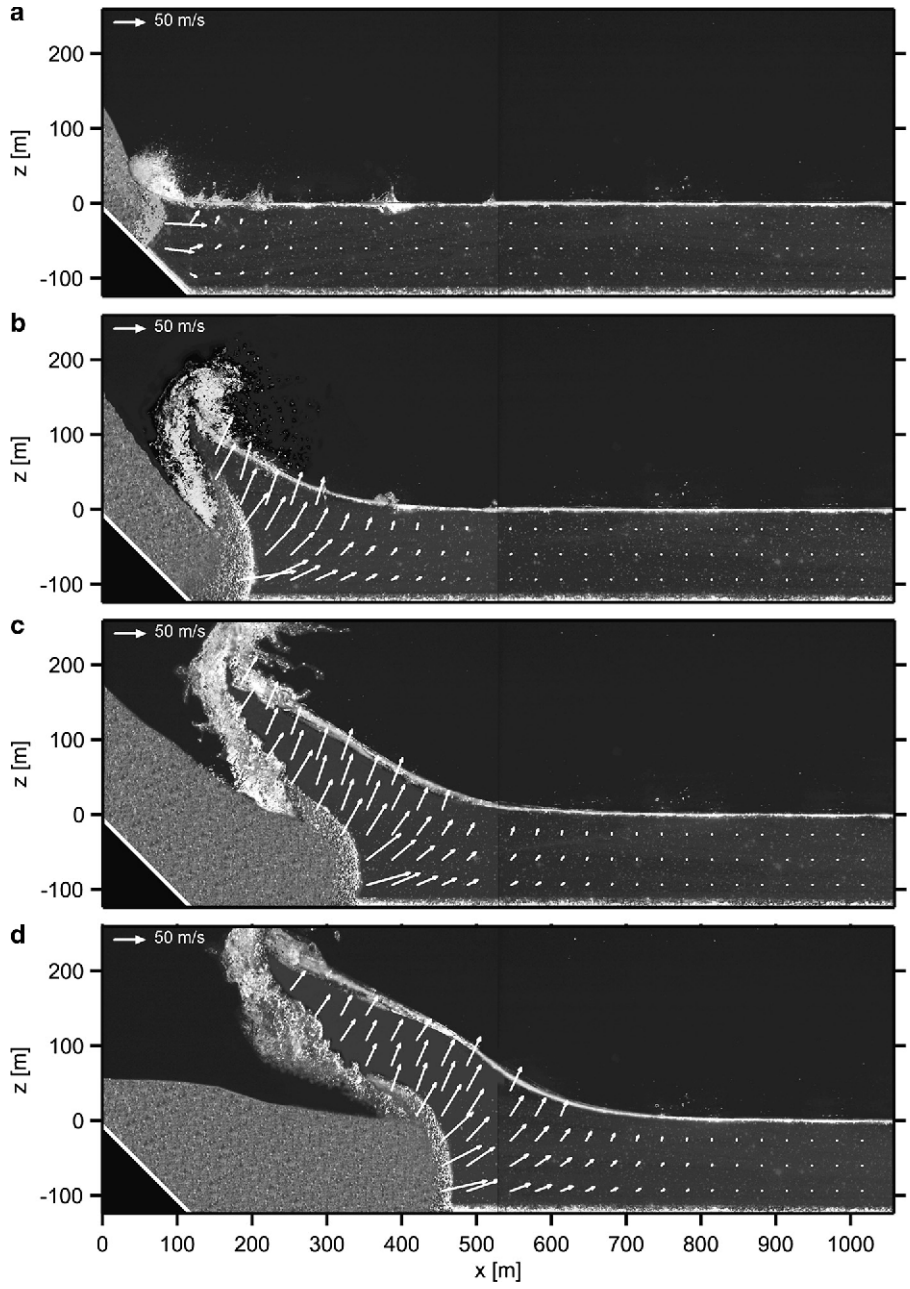

Figure 8
PIV velocity vector plot sequence of two synchronized granular slide impact experiments with juxtaposed areas of view and upscaled parameters: F = 3.18, v_s = 110 m/s, m' = 98.5 × 10^3 t/m′, h = 122 m, $\alpha = \beta = 45°$, time increment 1.73 s with first image at t = 0.76 s after impact.

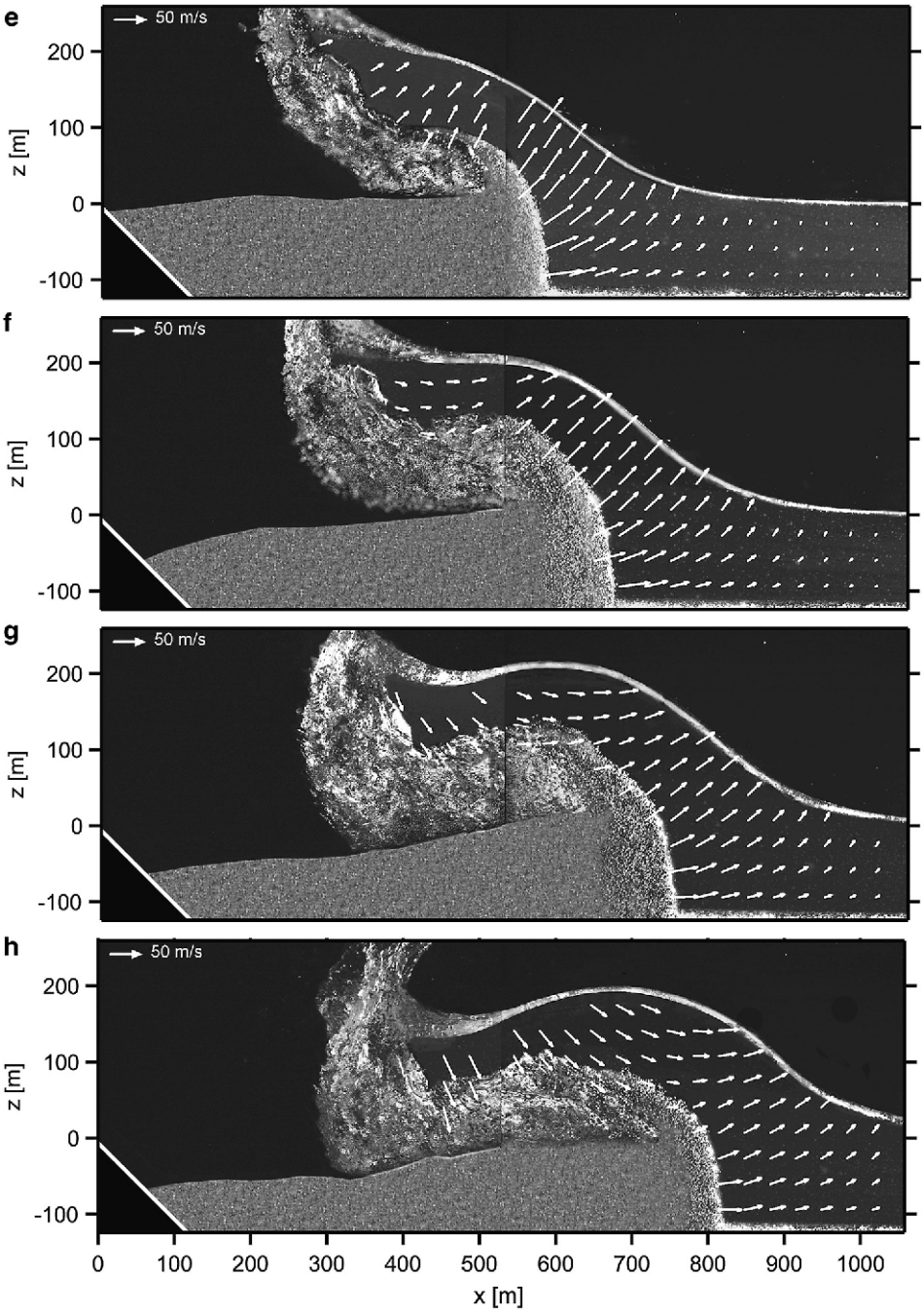

Figure 8
contd.

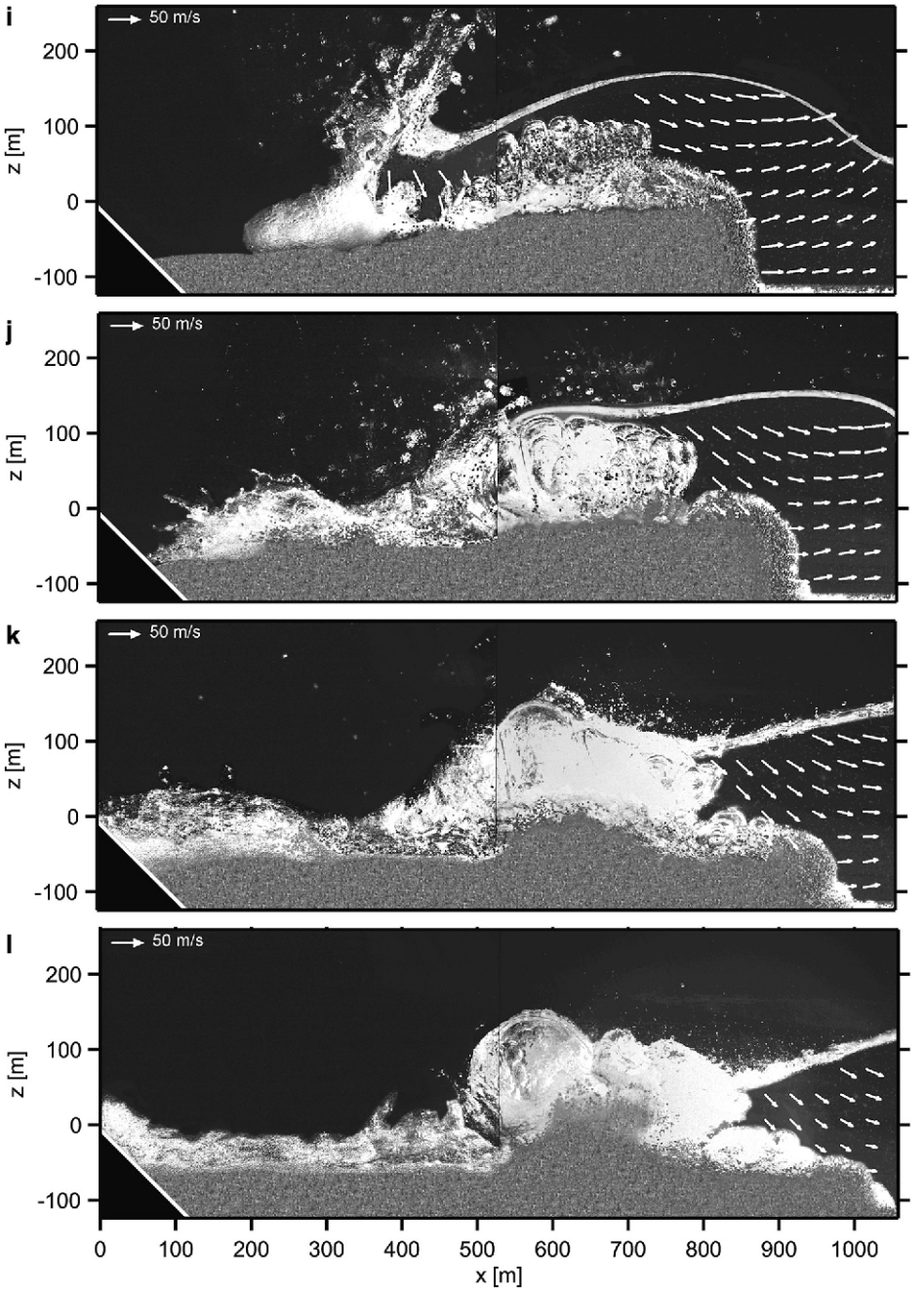

Figure 8
contd.

synchronously with the cavity collapse to a tsunami wave with $a = 152$ m at $t = 16$ s and $x = 885$ m (Fig. 7a). A high velocity gradient at the slide-water interface during impact and penetration causes sediment transport on the slide front leading to a sheet flow effect (Fig. 8b). The three phases — granular material, water and air — are clearly separated along distinct borderlines before flow reattachment occurs (Fig. 8h). Flow reattachment traps a large volume of air in the back of the landslide (Fig. 8i), which leads to large cavity formation (Fig. 8j), bubble break-up and massive phase mixing (Figs. 8k, l). Slide detrainment further increases phase mixing. The granular slide is deformed due to impact and deflection at the channel bottom reaching a maximum thickness and minimum length (Fig. 8d). The slide front forms an almost vertical wall with culminating height at the beginning of the cavity collapse (Figs. 8f, g). Thereafter the slide front thickness decays with slide run-out (Figs. 8j, k, l).

A sequence of eight PIV velocity vector plots acquired during tsunami runup on the headland is shown in Figure 9. The view area begins above the stillwater level. The sequence starts at $t = 23.28$ s after landslide impact and continues with a time step of

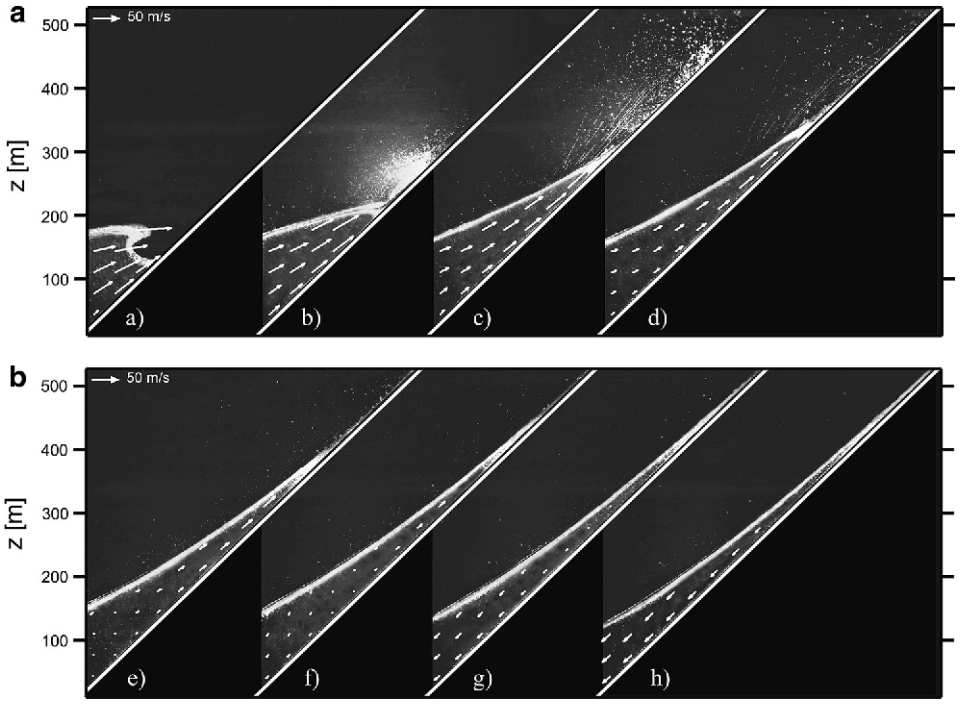

Figure 9
PIV velocity vector plot sequence of tsunami runup on headland slope created by a landslide impact with upscaled parameters: F = 3.18, $v_s = 110$ m/s, $m' = 98.5 \times 10^3$ t/m′, $h = 122$ m, $\alpha = \beta = 45°$, time increment 1.73 s, first image at $t = 23.28$ s after impact, lower left image corner at location $x = 1353$ m and $z = 11$ m.

1.73 s covering roughly a time span of 12 s. At $t = 23.28$ s the wave is shown prior to plunging onto the headland ramp. The wave amplitude has increased beyond 180 m. Wave-breaking during runup is initiated but does not fully develop due to the steep slope. The runup process is more surging than breaking and therefore with little air-entrainment (SYNOLAKIS, 1987; JENSEN *et al*., 2003). In the following images the wave surges up the headland slope with high velocity. At t = 30.2 s (Fig. 9e) an instantaneous stagnation point appears in the lower left corner of the velocity vector field. The stagnation point propagates up the headland ramp phase shifted to the runup wave front. In the area below the stagnation point water rushes down the headland ramp, whereas above the stagnation point water still surges upward. Therefore the sheet of water located on the headland ramp thinned significantly at the lower end by t = 35 s when the time of maximum runup height is reached (Fig. 9h). Sufficient water rushed up the headland slope to cause the flooding observed in Lituya Bay as estimated by MADER (1999) with numerical simulations of Lituya Bay outside the immediate impact area.

5. *Comparison with two-dimensional Predictive Models*

Various predictive relationships for the landslide-generated tsunami amplitude are compared with the Lituya Bay benchmark experiment as no field data are available on the tsunami height itself. Characteristic for highly non-linear waves is the large difference between the wave crest and the wave trough amplitudes. Predicting solely the total wave height H is insufficient and misleading (FRITZ *et al*., 2006). The comparison between the measured and predicted wave amplitudes and heights using the various equations is shown in Table 1.

The equation by FRITZ *et al*. (2004) for the maximum leading crest amplitude matched the measured crest amplitude $a = 155$ m. The relationship presented by KAMPHUIS and BOWERING (1970) from tray impact experiments matched the measured wave height $H = 162$ m. NODA (1970) used linear wave theory to predict the form of the wave motion produced by a body falling vertically into a tank. The theoretical solution underestimates the maximum wave amplitude with $a = 122$ m by 20%. The linear solution does not distinguish between the wave crest and trough amplitudes. Hence the trailing wave trough is massively overestimated. NODA (1970) obtained a theoretical solution for the case of a horizontally penetrating wall, which overestimates the measured wave crest amplitude by a factor of three. Similar overestimations may be produced by depth averaging shallow water equations in the wave generation area (MADER, 1999). SLINGERLAND and VOIGHT (1982) derived an empirical regression from two case studies, which overestimate the measured wave height by a factor of two. The empirical formula of HUBER and HAGER (1997) for 2-D-impulse wave characteristics predicts a wave height of $H = 94$ m, which underestimates the wave height by a factor of 1.8. Rough estimations of slide thickness from photos (HUBER, 1980) indicate that Huber's slides at comparable impact Froude

Table 1

Lituya Bay 1958 benchmark comparison of wave amplitude and runup predictions

Reference	Equations and remarks	a_C [m]	a_T [m]	H [m]	R [m]
Fritz *et al.* (2001) (scale model case study)	measured	152	10	162	530
Fritz (2002); Fritz *et al.* (2004) (granular slide model)	$\frac{a_C}{h} = 0.25\left(\frac{v_s}{\sqrt{gh}}\right)^{1.4}\left(\frac{s}{h}\right)^{0.8}$	155			
Huber and Hager (1997) (granular slide model)	$H = 0.88\sin\alpha\left(\frac{\rho_s}{\rho_w}\right)^{1/4}\left(\frac{V_s}{b}\right)^{1/2}\left(\frac{h}{x}\right)^{1/4}$			94	
Kamphuis and Bowering (1970) (block/weighted tray model)	$\frac{H}{h} = \left(\frac{v_s}{\sqrt{gh}}\right)^{0.7}\left(0.31 + 0.2\log\left(\frac{l_s s}{h^2}\right)\right) + 0.35e^{-0.08(x/h)}$			159	
Noda (1970) (theoretical solution)	$\frac{\eta(x,t)}{s} = f\left(\frac{v_s}{\sqrt{gh}}, \frac{x}{h}\right)$	122			
Noda (1970) (piston model)	$\frac{a_C}{h} = 1.32\left(\frac{v_s}{\sqrt{gh}}\right)$	515			
Slingerland and Voight (1982) (granular bag model)	$\log\left(\frac{a_C}{h}\right) = -1.25 + 0.71\log\left(\frac{1}{2}\frac{\rho_s}{\rho_w}\frac{V_s}{h^3}\frac{v_s^2}{gh}\right)$	329			
Mader and Gittings (2002)	full Navier-Stokes numerical simulation	170			580
Hall and Watts (1953) (R only based on measured H by Fritz *et al.*, 2001)	$\frac{R}{h} = 3.1\left(\frac{H}{h}\right)^{1.15}$				526
Synolakis (1987) (R only based on measured H by Fritz *et al.* 2001)	$\frac{R}{h} = 2.831\sqrt{\cot\beta}\left(\frac{H}{h}\right)^{5/4}$				493

numbers were thinner $s < h$. The present study and the sliding block experiments conducted by Noda (1970) and Kamphuis and Bowering (1970) showed a strong dependency of the generated wave heights on the slide impact thickness and the slide Froude number $F = v_s/(gh)^{0.5}$. The relationship given by Fritz *et al.* (2004) is recommended to predict the maximum leading crest amplitude a, because the relationship presented by Kamphuis and Bowering (1970) allows only the prediction of the total wave height H. The Lituya bay cross section was modeled numerically by Mader and Gittings (2002), Quecedeo *et al.* (2004) and Weiss and Wuennemann (2007) with full Navier-Stokes hydrodynamic codes in two dimensions. Both the Hall and Watts (1953) and Synolakis (1987) solutions for solitary wave runup on an impermeable slope match the experimentally measured wave runup and the observed elevation of forest destruction in Lituya Bay with predictions of $R = 526$ m and $R = 493$ m based on the experimentally measured incident wave parameters $H = 162$ m and $h = 122$ m (Fritz *et al.*, 2001). This confirms the conclusion drawn by Slingerland and Voight (1979) using back-calculation of wave height from runup that a wave height of about 160 m was necessary to produce the wave runup in Gilbert Inlet.

6. Three-dimensional Landslide Tsunami Experiments

The coupling between landslide motion and three-dimensioinal tsunami wave propagation and runup is of critical importance given the local, strongly-directional source mechanism. A unique pneumatic landslide generator was designed by the authors at Georgia Tech and installed at the NEES Tsunami Wave Basin (TWB) at OSU as shown in Figure 10. The apparatus simulated the impact of landslides that occur both above and below the water's surface. The landslide tsunami generator was constructed as an open aluminum box that is mounted on a steel slide and filled with up to 1,350 kg of gravel. The box accelerates down the slide by means of four pneumatic pistons. The granular mass is accelerated inside the box and released by opening the front tarp while the sled is slowed down pneumatically. The box measures 2.1 m by 1.2 m by 0.3 m with subdivisions to adjust initial slide length and thickness, and is placed on a slide that can vary in length. The box itself is able to travel approximately 2 m before the gravel is released down the 2H:1V slope at initial velocities up to 5 m/sec. Using cameras placed above and within the water, the researchers measured the shape, length, and thickness of the gravel masses while they were in motion.

The measured front velocity of the granular landslide and the corresponding acceleration are shown in Figure 11. The landslide velocity prior to release from the box is measured using the string pot data from the slide box. The landslide velocity after release from the box is measured from the image sequences recorded by a 2-megapixel PIV camera. The impact velocity of the landslide is compared to the velocity evolution of a dry granular landslide run. The PIV camera is setup at a distance of 6.8 m perpendicular to the hill slope providing an approximate 15 m^2 (4.5 m by 3.38 m) view area. A characteristic image sequence is shown in Figure 11b. This image sequence highlights the lateral spreading of the granular landslide after exiting the slide box prior to impact on

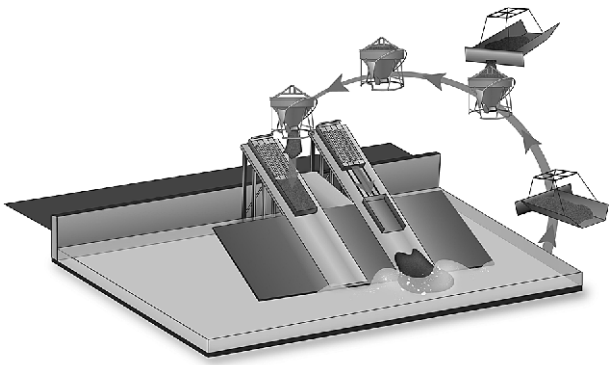

Figure 10
Granular landslide tsunami generator deployed in the three-dimensional NEES Tsunami Wave Basin at OSU in 2006/2007.

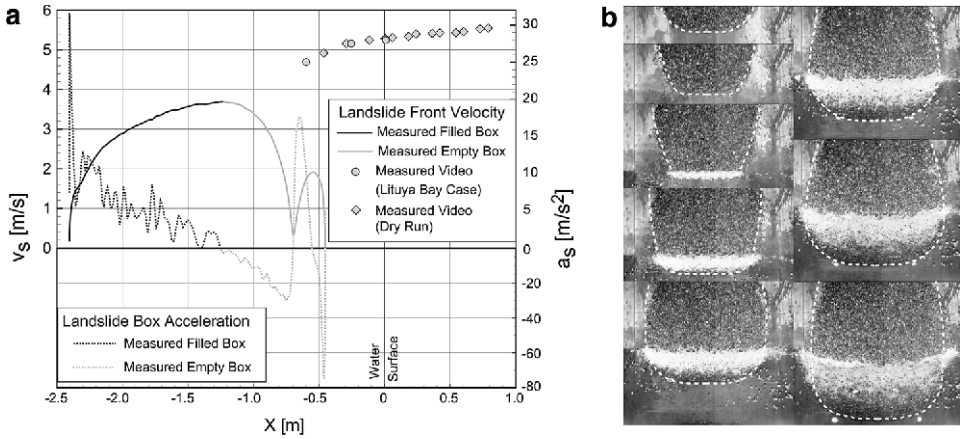

Figure 11
Granular Landslide kinematics at F = 3.2: (a) granular landslide front kinematics with transition from pneumatic acceleration inside the landslide generator to subaerial gravity slide; (b) lateral spreading and deformation of the granular landslide on the hill slope in a video image sequence.

the water body. The landslide shape is geometrically similar to the Lituya Bay landslide shown in Figure 2 at a 1:400 scale. The granular landslide front velocity prior to impact on the water surface was calculated from recorded subaerial landslide shown in Figure 11a. At the impact, a landslide velocity of 5.26 m/s was measured, which corresponds to an impact slide Froude number of 3.07 based on a still water depth 0.3 m and the definition $F = v_s/(gh)^{1/2}$. This corresponds to a full three- dimensional physical model of the Lituya Bay landslide at a 1:400 scale. Hence the pneumatic landslide generator can reproduce landslide velocities scaled to real world physical events.

The recorded high-resolution image sequences were processed with PIV to analyze the landslide characteristics at the impact location and the wave generation process by measuring the surface velocity field. The speckle patterns generated by the landslide granulate surface were used for iterative multi-pass cross-correlation analysis with decreasing window sizes down to 32 by 32 pixels. A PIV velocity vector plot of the landslide surface shortly after impact corresponding to a 1:400 scale landslide model of the three-dimensional Lituya Bay landslide is shown in Figure 12a. The landslide front penetrated below the water surface enabling the PIV based analysis of the water surface in the impact zone, which was seeded with 5 mm diameter naturally buoyant tracer particles prior to each experiment. The granular landslide deposits were scanned with an acoustic multi-transducer array (Fig. 12b). Unfortunately the Lituya Bay landslide deposit has not been surveyed to date, which would be necessary to compare physical model results with the landslide deposits in the field. The proposed landslide deposit mapping was conducted, for example, in Lake Lucerne, Switzerland (SCHNELLMANN *et al.*, 2002).

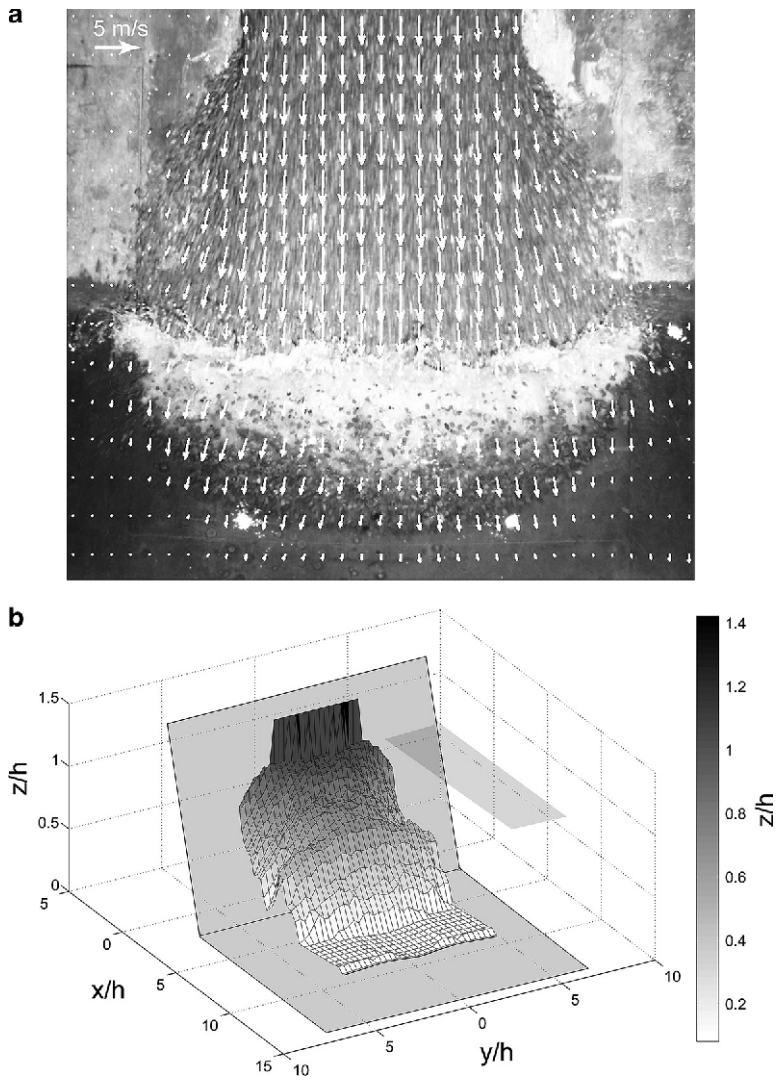

Figure 12
Landslide tsunami generation in 3-D: (a) PIV velocity vector plot of the landslide surface shortly after impact with the landslide front penetrating below the water surface and tsunami wave generation (note: the displayed number of vectors is reduced for visibility); (b) granular landslide deposit scanned with an acoustic multi-transducer array.

Wave gauges were placed to measure the size and shape of the tsunami waves that were generated, including the lateral onshore runup. The locations of wave and runup gauges in the tsunami wave basin measuring 48.8 m by 26.5 m by 2.1 m (L $\times$ W $\times$ H) at OSU are shown in Figure 13a. The scaled gauge locations are based on a 0.3 m water depth, which corresponds to a 1:400 scale model given the 122 m water depth at the

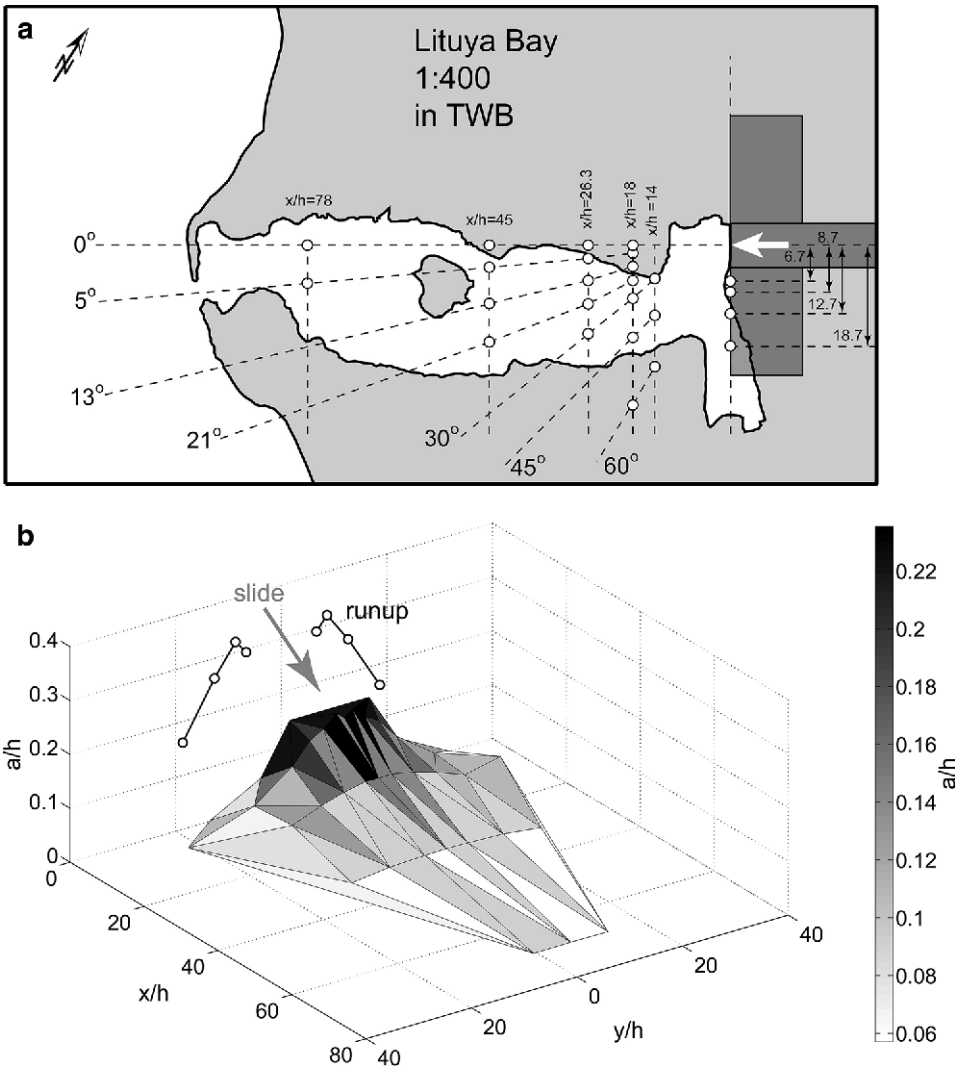

Figure 13
Landslide tsunami propagation in 3-D: (a) Locations of wave and runup gauges in tsunami wave basin at OSU based on a 1:400 scale Lituya Bay water depth with superimposed Lituya Bay coastline for reference; (b) tsunami amplitude attenuation with strong directional component and the high wave runup as edge waves along the hill slope.

impact site in Lituya Bay. The scaled Lituya Bay coastline is superimposed to highlight the complicated setting. The detailed fully three-dimensional bathymetry and topography of Lituya Bay would have to be reconstructed in the physical model to enable a direct comparison between the measurements and the observations in the field. The tsunami amplitude attenuation and the wave runup along the hill slope are shown in Figure 13b.

The recorded wave profiles were extremely directional, unsteady, nonlinear, and located mostly in the intermediate water depth wave regime. Among the principal differences between a tectonic-generated tsunami and a landslide-generated tsunami is that the latter has a strong directional component that can be devastating to the immediate area. Because it has a shorter wavelength, however, it dissipates quickly over a short distance. Landslide tsunamis exhibit a more dispersive and strongly directional propagation than tectonic tsunamis. Currently more than 60 successful runs have been completed and the main tsunamigenic parameters identified that will serve as key benchmarks for numerical models. However a fully three-dimensional benchmark of the Lituya Bay with the detailed bathymetry remains to be conducted to validate numerical simulations of the entire Lituya Bay with three-dimensional tsunami generation, propagation and runup.

7. Conclusions

The two-dimensional physical model at 1:675 scale of the Lituya Bay 1958 event includes landslide impact, tsunami generation, propagation and runup on headland. A unique pneumatic landslide generator was used to generate a high-speed granular slide with controlled impact velocity and shape. State-of-the-art laser measurement techniques such as particle image velocimetry (PIV) and laser distance sensors (LDS) were applied to cope with an extremely unsteady three phase flow due to high speed granular slide impact, high velocity gradients, flow separation, cavity formation, wave generation and runup. A granular slide with density and volume given by MILLER (1960) impacting at a mean velocity of 110 m/s generates a large air cavity and an extremely nonlinear wave beyond breaking criterion, which remains nonbreaking due to the short propagation distance to the headland runup. The formation of a large air cavity is highlighted (FRITZ *et al*., 2001). The predictive tsunami amplitude equation by FRITZ *et al*. (2004) matches the experimentally measured tsunami amplitude in Gilbert Inlet. The experimentally measured wave runup matches the trimline of forest destruction on the spur ridge in Gilbert Inlet. Back-calculations of wave height from observed trimline of forest destruction using HALL and WATTS (1953) and SYNOLAKIS (1987) runup formulas equal the measured wave height in Gilbert Inlet. Further research on slide impact characteristics, wave generation and energy conversion using three-dimensional models is necessary. MADER and GITTINGS (2002), QUECEDO *et al*. (2004) as well as WEISS and WUENNEMANN (2007) reproduced the physical model results of the Lituya Bay landslide tsunami with full Navier-Stokes models in two dimensions. A three-dimenional pneumatic landslide tsunami generator was designed, constructed and successfully deployed in the tsunami wave basin at OSU. The Lituya Bay landslide was reproduced in a three-dimensional physical model at 1:400 scale. The landslide surface velocities distribution was measured with PIV. The landslide deposits in Lituya Bay should be mapped to validate the experiments and establish a baseline bathymetry prior to a possible future landslide tsunami in Lituya Bay. A detailed three-dimensional benchmark experiment of the Lituya

Bay remains to be conducted with the exact bathymetry to validate numerical simulations of the entire Bay with three-dimensional tsunami generation, propagation and runup.

Acknowledgments

This research work is supported by the National Science Foundation under Grant No. CMS-0421090. Any opinions, findings, and conclusions or recommendations expressed herein are those of the author(s) and do not necessarily reflect the views of the National Science Foundation. The two-dimensional experiments conducted at VAW (ETH Zürich) were supported by the Swiss National Science Foundation, grant number 2100-050586.97.

References

Dean, R.G. and Dalrymple, R.A., *Water wave mechanics for engineers and scientists. Advanced Series on Ocean Engineering* 2 (World Scientific, Singapore 1991).

Fritz, H.M., Hager, W.H. and Minor, H.-E. (2001), *Lituya Bay case: rockslide impact and wave runup*, Science of Tsunami Hazards *19*(1), 3–22.

Fritz, H.M., *PIV applied to landslide generated impulse waves*, In (Adrian, R.J. *et al*., eds) *Laser Techniques for Fluid Mechanics*, pp. 305–320 (Springer, New York, Berlin, Heidelberg 2002a).

Fritz, H.M., *Initial phase of landslide generated impulse waves*, In (Minor, H.-E., ed.) *VAW Mitteilung 178* (Versuchsanstalt für Wasserbau, Hydrologie und Glaziologie, ETH Zürich 2002b).

Fritz, H.M. and Moser, P. (2003), *Pneumatic landslide generator*. Int. J. Fluid Power *4*(1), 49–57.

Fritz, H.M., Hager, W.H. and Minor, H.-E. (2003a), *Landslide generated impulse waves, Part 1: Instantaneous flow fields*, Exp. Fluids *35*, 505–519.

Fritz, H.M., Hager, W.H., and Minor, H.-E. (2003b), *Landslide generated impulse waves, Part 2: Hydrodynamic impact craters*, Exp. Fluids *35*, 520–532.

Fritz, H.M., Hager, W.H., and Minor, H.-E. (2004), *Near field characteristics of landslide generated impulse waves*, J. Waterway, Port, Coastal, and Ocean Engrg., ASCE *130*, 287–302.

Fritz, H.M., Physical modeling of landslide generated tsunami. In (A. Mercado-Irizarry and P.L.-F. Liu, eds) *Caribbean Tsunami Hazard* (World Scientific, Singapore 2006), pp. 308–324.

Hall, J.V., Jr. and Watts, G.M. (1953), *Laboratory investigation of the vertical rise of solitary waves on impermeable slopes*, Tech. Memo *33*, U.S. Army Corps of Engineers, Beach Erosion Board.

Hart, D., *PIV error correction*. In *Laser Techniques Applied to Fluid Mechanics*, selected papers from the 9th Internat. Symp., Lisbon 1998, Portugal. (Eds. Adrian, R.J. *et al*.) (Springer, New York 2000).

Heller, V., Hager, W.H., and Minor, H.-E. (2008), *Scale effects in subaerial landslide generated impulse waves*, Exp. Fluids *44*(5), 691–703, doi:10.1007/s00348-007-0427-7.

Huber, A., *Schwallwellen in Seen als Folge von Bergstürzen* (in German), *VAW-Mitteilung 47*, (Ed. Vischer, D.) (Versuchsanstalt für Wasserbau, Hydrologie und Glaziologie, ETH Zürich 1980).

Huber, A. and Hager, W.H. (1997), *Forecasting impulse waves in reservoirs. Dix-neuvième Congrès des Grands Barrages* C31:993–1005. Florence, Italy. Commission International des Grands Barrages, Paris.

Jensen, A., Pedersen, G.K., and Wood, D.J. (2003), *An experimental study of wave runup at a steep beach*, J. Fluid Mech. *486*, 161-188, doi:10.1017/S0022112003004543.

Jørstad, F. (1968), *Waves generated by landslides in Norwegian fjords and lakes*. Norwegian Geotechnical Institute Publication *79*:13–32, Norwegian Geotechnical Institute, Oslo.

Kamphuis, J.W. and Bowering, R.J. (1970), *Impulse waves generated by landslides*. In *Proc. 12th Coastal Engin. Conf.* ASCE *1*, 575–588.

LAW, L. and BREBNER, A. (1968), *On water waves generated by landslides*, *3rd Australas. Conf. on Hydraulics and Fluid Mechanics*, Sydney, Paper *2561*, 155–159.

MADER, C.L. (1999), *Modelling the 1958 Lituya Bay mega-tsunami*. Science of Tsunami Hazards *17*(2), 57–67.

MADER, C.L. and GITTINGS, M.L. (2002), *Modeling the 1958 Lituya Bay mega-tsunami, II*. Science of Tsunami Hazards *20*(5), 241–250.

MILLER, D.J. (1960), *Giant waves in Lituya Bay, Alaska*, Geological Survey Professional Paper *354*-C, U.S. Government Printing Office, Washington D.C.

MÜLLER, D., *Auflaufen und Überschwappen von Impulswellen an Talsperren* (in German). *VAW-Mitteilung* 137 (Ed. Vischer, D.) (Versuchsanstalt für Wasserbau, Hydrologie und Glaziologie, ETH Zürich 1995).

MÜLLER, L. (1964), *The rock slide in the Vajont Valley*. Rock Mech. Eng. Geol. *2*(3–4), 148–212.

Noda, E. (1970), *Water waves generated by landslides*, J. Waterw. Harbors Coastal Eng. Div. ASCE *96*(WW4), 835–855.

PARARAS-CARAYANNIS, G. (1999), *Analysis of mechanism of tsunami generation in Lituya Bay*, Science of Tsunami Hazards *17*(3), 193–206.

QUECEDO, M., PASTOR, M., and HERREROS, M.I. (2004), *Numerical modelling of impulse wave generated by fast landslides*, Int. J. Numer. Meth. Engin. *59*, 1633–1656. doi: 10.1002/nme.934.

SAVAGE, S.B. (1979), *Gravity flow of cohesionless granular materials in chutes and channels*, J. Fluid Mech. *92*, 53–96.

SCARANO, F. and RIETHMULLER, M. (1999), *Iterative multigrid approach in PIV image processing with discrete window offset*, Experiments in Fluids *26*, 513–523.

SCHNELLMANN, M., ANSELMETTI, F.S., GIARDINI, D., MCKENZIE, J.A., and WARD, S.N. (2002), *Prehistoric earthquake history revealed by lacustrine slump deposits*, Geology *30*(12), 1131–1134.

SHARPE, C.F.S., *Landslides and Related Phenomena* (Columbia Univ. Press, New York 1938).

SLINGERLAND, R.L. and VOIGHT, B., *Occurrences, properties and predictive models of landslide-generated impulse waves*, Rockslides and Avalanches *2*, 317–397 (Ed. Voight, B) *Developments in Geotechnical Engin.* 14B (Elsevier, Amsterdam 1979).

STIVE, M.J.F. (1985), *A scale comparison of waves breaking on a beach*, Coastal Engin. *9*, 151–158.

Synolakis, C.E. (1987), *The runup of solitary waves*, J. Fluid Mech. *185*, 523–545.

TOCHER, D. and MILLER, D.J. (1959), *Field observations on effects of Alaskan earthquake of 10 July, 1958*, Science *129*, 394–395.

TOGNACCA, C., *Beitrag zur Untersuchung der Entstehungsmechanismen von Murgängen (in German)*, *VAW-Mitteilung* 164 (Ed. Minor, H.-E.) (Versuchsanstalt für Wasserbau, Hydrologie und Glaziologie, ETH Zürich 1999).

VARNES, D.J. (1958), *Landslide types and processes*, Highw. Res. Board Spec. Rep. *29*, Natl. Acad. Sci.-Natl. Res. Counc. Publ. *544*, 22–47.

VOIGHT, B., JANDA, R.J., GLICKEN, H., and DOUGLASS, P.M. (1983), *Nature and mechanics of the Mount St. Helens rockslide-avalanche of 18 May 1980*, Géotechnique *33*, 243–273.

WEISS, R. and WUENNEMANN, K. (2007), *Understanding tsunami by landslides as the next challenge for hazard, risk and mitigation: Insight from multi-material hydrocode modeling*, EOS Trans. AGU *88*(52), Fall Meet. Suppl., Abstract S51C-06.

WIEGEL, R.L., *Oceanographical Engineering* (Prentice-Hall, Englewood Cliffs, N.J. 1964).

(Received December 31, 2007, revised September 2, 2008)
Published Online First: February 6, 2009